Segmentation of Focal Brain Lesions

Frithjof Kruggel

Interdisziplinäres Zentrum für Klinische Forschung (IZKF),
Inselstrasse 22, D-04103 Leipzig, Germany
kruggel@cbs.mpg.de

Abstract. Focal brain lesions are a consequence of head trauma, cerebral infarcts or intracerebral hemorrhages. In clinical practice, magnetic resonance imaging (MRI) is commonly used to reveal them. The segmentation task consists of finding the lesion borders. This problem is non-trivial because the lesion may be connected to other intracranial compartments with similar intensities. A new method for the automatic segmentation of unilateral lesions is proposed here. The signal statistics of multichannel MR are examined w.r.t. the first-order mirror symmetry of the brain. The algorithm is discussed in detail, and its properties are evaluated on synthetic and real MRI data.

1 Introduction

High resolution magnetic resonance (MR) images of the brain are used in clinical practice to reveal focal brain lesions (e.g., as consequences of head trauma, intra-cerebral hemorrhages or cerebral infarcts). Lesion properties (i.e., position, extent, density) are known to be related to cognitive handicaps of a patient. While a *semi-quantitative* analysis of MR tomograms based on visual inspection (e.g., rating scales) is common today in certain clinical protocols, tools for a *quantitative* analysis are still rare. One of the reasons for this lack of tools is that segmenting MR images with pathological findings is considered a non-trivial task.

Manual lesion segmentation is still considered as the "gold standard". A human expert with anatomical knowledge, experience and patience uses some graphical software tool to outline the region of interest. While this method obviously produces the most reliable results, it is time consuming and tedious. In addition, re-tests and inter-rater reliability studies of manually segmented lesion rarely reach 90 % correspondence [2], [21]. Most previous studies in automatical lesion segmentation concentrated on the detection of white matter lesions in Multiple Sclerosis (MS). Techniques suggested for this problem include: statistical clustering [19], a combination of statistical techniques and anatomical knowledge [7], a combined classification of multi-channel MR images [22] or an iterative approach to correct B_1 field inhomogeneities while classifying voxels [11]. However, the problem studied in this paper is more general. While MS lesions are completely caused by white matter, lesions as consequences of a head trauma or cerebral infarction may include the cortical gray matter and thus reach the cerebrospinal fluid (CSF) compartment. So the problem is to discriminate a lesion from *different* surrounding compartments.

G.-Z. Yang and T. Jiang (Eds.): MIAR 2004, LNCS 3150, pp. 10–18, 2004.

Few semi-automatic and automatic methods exist in the literature for this problem. Most are dedicated to the segmentation of a specific type of focal lesion only. Maksimovic *et al.* [14] studied the segmentation of fresh hemorrhagic lesions from CT data using 2D active contours. Such lesions have high signal intensities and may reach the skull which is also bright. The active contour detects the border between the brain and the skull, the boundary of the ventricles and the boundary of the lesion. Loncaric *et al.* [12], [13] proposed an approach that combines unsupervised fuzzy clustering and rule-based system labeling. The rule-based system assigns one of the following labels to each region provided by the clustering: background, skull, brain, calcifications and intracerebral hemorrhages.

Dastidar *et al.* [3] introduced a semi-automatic approach for segmenting infarct lesions consisting of four steps: image enhancement, intensity thresholding, region growing and decision trees in order to localize the lesion. User interaction is required to define the lesion boundaries if it reaches a compartment of similar intensity. Stocker *et al.* [17] proposed to automatically classify multichannel image information (T_1-, T_2- and proton density (PD)) using a a self-organizing map into five partitions: white and gray matter, CSF, fluid and gray matter in the infarct region. Brain tumors may be segmented using statistical classification [8], [15]. An atlas of normal brain anatomy containing spatial tissue probability information is used to discriminate different anatomical structures with similar intensities. A tumor is found as a (compact) region of outlier voxels.

A level-set method guided by a tumor probability map was described by Ho *et al.* [4]. Finally, a region growing technique was proposed to segment any type of lesions [18]. It requires the input of a seed point and a pre-defined threshold to avoid an overgrowing outside the lesion. A similar method was developed by Hojjatoleslami *et al.* [5], [6]. The key idea is to stop the region growing on the outer cortical layer between the lesion and the external CSF area, that is often preserved after stroke. The algorithm involves a grey level similarity criterion to expand the region and a size criterion to prevent from overgrowing outside the lesion.

In this paper, we focus on the segmentation of unilateral focal brain lesions in their chronic stage. Lesions are generally not homogeneous, often with completely damaged core parts and minor damage in peripheral portions. Thus, MR signal intensities range between values of undamaged tissue and values similar to CSF. The boundary between a cortical lesion and the CSF compartment is often hard to draw.

The following section of this paper describes the method. In a subsequent section, we study the parameter settings and performance of our method by several exeriments. Finally, properties of this approach are summarized.

2 The Algorithm

As a first approximation, the brain is a mirror-symmetric organ. Lesions considered here are confined to a single hemisphere with a generally healthy area on the contralateral side (see Fig. 1. The segmentation problem may therefore be stated as finding compact areas with an intensity statistic that differs significantly from the contralateral side. A Hotelling T^2 test is performed to compare small subregions from both hemispheres. The test measure is converted into a z-score and collected in a lesion probability map (LPM).

Areas with high signal asymmetries are depicted by high z-scores. A post-processing step thresholds the LPM and checks the size of all connected regions against the size distribution of natural asymmetries.

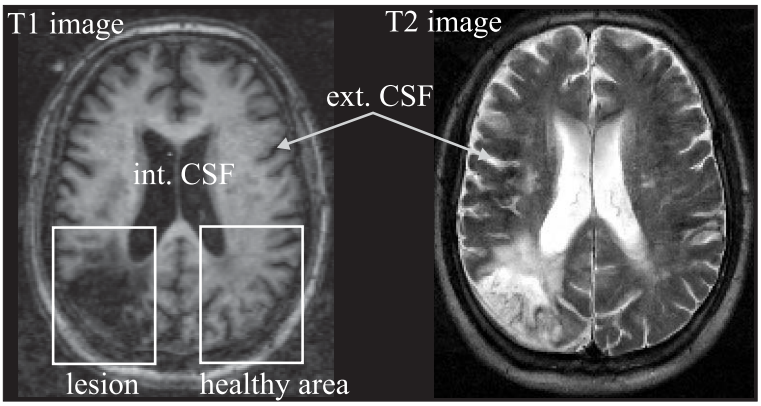

Fig. 1. Lesions considered here are confined to a single hemisphere with a generally healthy area on the corresponding contralateral side

2.1 Computing a Lesion Probability Map

To detect a probable lesion, we compare the signal statistics in homologeous regions of both brain hemispheres in multichannel MRI tomograms. As a pre-processing step, we align brain datasets with the stereotactical coordinate system such that the midsagittal plane is at a known location $x_{mid} = const$. We use a natural convention for addressing the body side, i.e. locations $x_l < x_{mid}$ refer to the left body side. Now consider a cubic subregion R in the left brain hemisphere centered around a voxel v_l at Cartesian coordinates (x_l, y, z) with an extent of s voxels. Its homologeous region is centered around voxel v_r at $(2 * x_{mid} - x_l, y, z)$. At each voxel v, a vector of observed signal intensities $\mathbf{o}_k = \{o_1, \ldots, o_k\}$ is obtained from the k multichannel images. Thus, a region includes $n = s^3$ observation vectors.

We are now interested whether the multivariate mean of observations in both regions is different. Hotelling's T^2 statistic is an important tool for inference about the center of a multivariate normal quantity. According to Rencher [16], we can work directly with the differences of the paired observations from both hemispheres, i.e. reduce the problem to a one-sample test for $D_n = \{\mathbf{d_1}, \ldots, \mathbf{d_n}\}$ from $N_k(\bar{\mathbf{d}}, \mathbf{\Sigma})$, where $\mathbf{d_i} = \mathbf{o_{l,i}} - \mathbf{o_{r,i}}$ correspond to the left-right differences, and $\bar{\mathbf{d}}, \mathbf{\Sigma}$ are unknown. The hypothesis $H_0 : \bar{\mathbf{d}} = 0$ is rejected at the level α if

$$T^2 := n\bar{\mathbf{d}}^{\mathsf{T}}\mathbf{S}^{-1}\bar{\mathbf{d}} > \frac{(n-1)k}{(n-k)}\, F_{k,n-k,1-\alpha}, \tag{1}$$

where

$$\bar{\mathbf{d}} = \frac{1}{n}\sum_{i=1}^{n}\mathbf{d}_i \quad \text{and} \quad \mathbf{S} = \frac{1}{n-1}\sum_{i=1}^{n}(\mathbf{d_i} - \bar{\mathbf{d}})(\mathbf{d_i} - \bar{\mathbf{d}})^{\mathsf{T}} \tag{2}$$

are the mean and the covariance of the sample. Obtained $F_{k,q}$-scores are converted into significance levels p [1]:

$$p \in [0,1] = 2\,I_x\left(\frac{k}{2},\frac{q}{2}\right), \quad \text{where} \quad x = \frac{q}{q+kF}, \tag{3}$$

and $I_x(\cdot)$ corresponds to the incomplete beta function [1]. Significance levels are finally converted into z-scores:

$$z = \sqrt{2}\,\mathrm{erfc}^{-1}(p/2), \quad p \in [0,1]. \tag{4}$$

Z-scores are compiled in a statistical image that we denote as LPM. Note that this map is symmetric with respect to the midsagittal plane.

2.2 A Weighted Hotelling T^2 Test

In order to obtain a more localized LPM, we include weights w_i with differences $\mathbf{d_i}$. The highest weight is addressed to the center voxel v_c of the subregion R. Weights decrease with distance from this voxel. A reasonable choice is a Gaussian weighting function:

$$w_i = \exp\left(-\frac{||v_i - v_c||^2}{2\sigma^2}\right), \quad v_i, v_c \in R, \tag{5}$$

where $||v_i - v_c||$ denotes the Euclidean distance between v_i and v_c and σ is a spatial scaling factor. Note that $\sigma \to \infty$ approaches the unweighted case above. Now, the weighted sample mean and covariance are computed as:

$$\bar{\mathbf{d_w}} = \frac{\sum_{i=1}^{n} w_i\mathbf{d}_i}{\sum_{i=1}^{n} w_i} \quad \text{and} \quad \mathbf{S_w} = \frac{\sum_{i=1}^{n} w_i(\mathbf{d_i} - \bar{\mathbf{d}})(\mathbf{d_i} - \bar{\mathbf{d}})^{\mathsf{T}}}{\sum_{i=1}^{n} w_i - \sum_{i=1}^{n} w_i^2}. \tag{6}$$

As Willems *et al.* [20] discussed for the case of a robust (weighted) Hotelling test, the test statistic is now:

$$T_w^2 := n\bar{\mathbf{d_w}}^{\mathsf{T}}{\mathbf{S_w}}^{-1}\bar{\mathbf{d_w}} \approx fF_{k,q,1-\alpha}, \tag{7}$$

where f is a multiplication factor and q the modified degrees of freedom for the denominator of the F-distribution, given by:

$$f = E[T_w^2]\frac{q}{q-2} \quad \text{and} \quad q = 4 + \frac{2E^2[T_w^2](k+2)}{kVar[T_w^2] - 2E^2[T_w^2]}. \tag{8}$$

Since the mean and the variance of the T_w^2 distribution cannot be obtained analytically, we determined values of $E[T_w^2]$ and $Var[T_w^2]$ using Monte-Carlo simulations [20].

For a fixed dimension $k = 2$, we generated $m = 10^6$ samples $X_i; i = 1,\ldots,m$ from a $N_k(0,\mathbf{I}_k)$ Gaussian distribution. For each sample, $T_w^{2(i)}$ was determined by Eq.

7, using different region extents of $s = \{3, 5, 7\}$ voxels (corresponding to samples sizes of $n = \{27, 125, 343\}$) and different spatial scaling factors $\sigma = \{0.5, \ldots, 2.5\}$. The mean and variance of $T_w^{2^{(i)}}$ are given by:

$$\hat{E}(T_w^2) := \frac{1}{m} \sum_{i=1}^{m} T_w^{2^{(i)}} \quad \text{and} \quad \widehat{Var}(T_w^2) := \frac{1}{m-1} \sum_{i=1}^{m} (T_w^{2^{(i)}} - \hat{E}(T_w^2))^2. \tag{9}$$

Following [20], a smooth function was fit to a regression model, depending on the window size s and the spatial scaling factor σ. For the reduced degrees-of-freedom q, given $k = 2$, we modelled:

$$q = 4 + \frac{4}{t_3 - 1}, \tag{10}$$

and, likewise, for the multiplication factor f:

$$f = (t_2 + t_1 \sigma^{-t_0}) \frac{q}{q-2}. \tag{11}$$

Values for t_i are given in Tab. 1.

s	t_0	t_1	t_2	t_3
3	20.74224	0.481705	2.347796	1.17270
5	4.02456	4.242255	2.066018	1.00784
7	3.78378	14.393344	2.006746	1.01824

Table 1. Regression parameters t_i for computing the multiplication factor f and the reduced degrees-of-freedom q, given a window size s.

The lesion probability map (LPM) is thresholded by z_{lim}, and the size of the connected components is determined. Natural asymmetries occur in any brain, but they are generally small compared with a brain lesion. The distribution of "pseudo-lesions" due to brain asymmetry was sampled from 20 datasets of healthy subjects. The size of a probable lesion is compared with this distribution, and a p-value is addressed to each lesion for being a "true" lesion. The algorithm was implemented and evaluated using the BRIAN system [9].

3 Experiments

The first experiment was conducted in order to study the influence of the parameters window size s, spatial scaling factor σ, and z-score threshold z_{lim} on the estimated size of the detected lesion. Denote a contrast ratio of 1.0 as a complete lesion, 0 as undamaged tissue. Simulated datasets with a lesion size of $l = \{13^3, 27^3, 58^3\}$ voxels and a contrast ratio of $c = \{0.1, 0.8\}$ were generated. The lesion detection algorithm was run on these data using window sizes of $s = \{3, 5, 7\}$, and $\sigma = \{0.5, 1.0, 1.5, 2.0, 2.5\}$.

We found: (1) The larger the window size, the higher the z-scores. (2) The larger σ, the higher the z-scores. (3) The z-score range, in which the true lesion size was correctly estimated, decreases with increasing σ. (4) The z-score range, in which the true lesion size was correctly estimated, increases with increasing window size. The best compromise was found with $s = 5$, $\sigma = 1$, and $z_{lim} = 4.3$ (see Fig. 2).

As a second experiment, we examined the contrast ratio, for which at least 95% of the true lesion size was detected. For a small lesion (10^3 voxels), $c = 0.17$ (3% noise), $c = 0.28$ (6% noise), for a large lesion (30^3 voxels), $c = 0.09$ (3% noise), $c = 0.18$ (6% noise) was found. So, for realistic noise levels found in MRI datasets, lesions with a contrast ratio of at least 0.2 are expected to be detected with a size that is close to the real one.

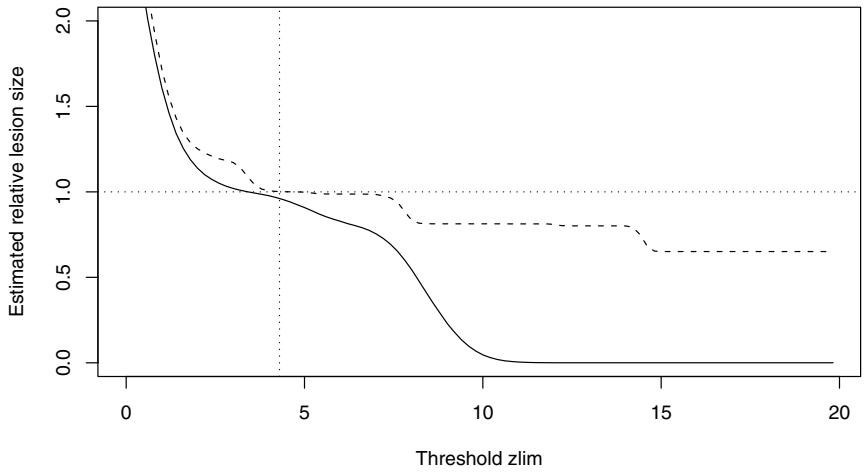

Fig. 2. Estimated relative size of the lesion vs. threshold z_{lim} for window size $w = 5$ and spatial scaling factor $\sigma = 1.0$. The solid line corresponds to a lesion contrast of 0.1, the broken line to a lesion contrast of 0.8.

Then, we were interested in discriminating real lesions from pseudo-lesions due to natural brain asymmetry which are expected to be small. We selected 20 datasets of healthy subjects from our brain database. A MDEFT protocol [10] was used to acquire high-resolution T_1-weighted data sets on a 3.0 Tesla Bruker Medspec 100 system (128 sagittal slices of 256*256 voxels, FOV 250 mm, slice thickness 1.4 mm, subsequent trilinear interpolation to an isotropic resolution of 1 mm). T_2-weighted datasets were collected on the same scanner (20 slices of 256*256 voxels of 0.97*0.97*7 mm). The T_1-weighted dataset was aligned with the stereotactical coordinate system, and the T_2-weighted dataset was rigidly registered with the aligned dataset using a multi-resolution approach and a cost function based on normalized mutual information. Then, the lesion segmentation algorithm was applied to the multichannel image, and the size of the de-

tected pseudo-lesions determined using $z_{lim} = 10$. In total, 2077 regions were found, and from their cumulative distribution function, a lesion of more than 880 voxels may be called pathological with an error of 5%.

Finally, we illustrate the use of this algorithm in a real dataset. A patient suffering from a stroke in the left anterior area of the middle cerebral artery was examined 6 months post-stroke (see Fig. 3). Note that not only the lesion itself is detected but also other areas (i.e., the left ventricle) are marked where some substance loss occured in the vicinity. Thus, all consequences of the stroke are depicted. Note further that low-intense regions in the vicinity of the Sylvian fissure are not included in the lesion, because they are symmetric.

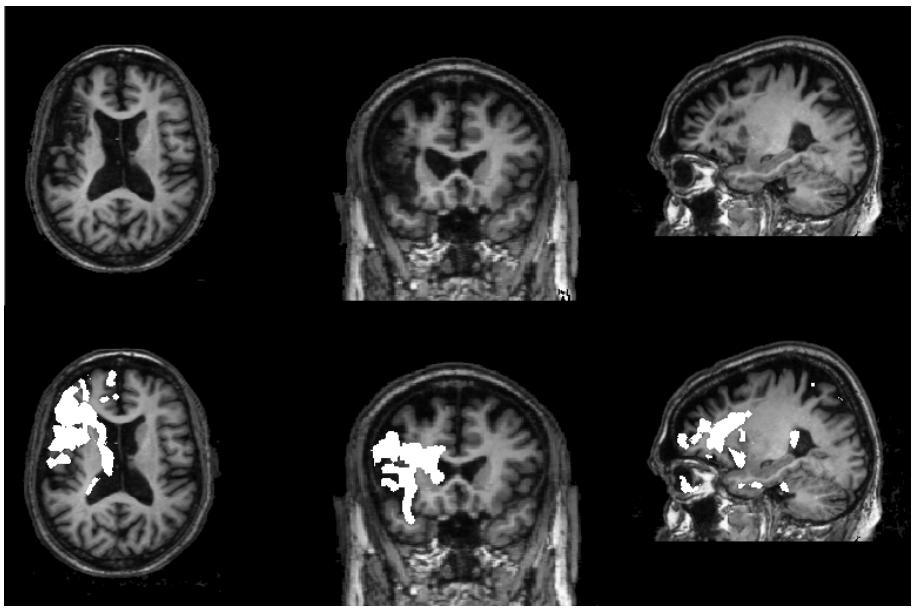

Fig. 3. Top: T_1-weighted image of a patient suffering from a cerebral infarction in the anterior supply area of the middle cerebral artery. Below: segmented lesion as detected by this algorithm.

4 Summary

We described an algorithm for detecting unilaterial focal lesions in MR images of the human brain. The signal statistic of small mirror-symmetric subregions from both hemispheres is compared using a spatially weighted Hotelling T^2 test. The resulting voxel-wise test measure is converted to a z-score and collected in a lesion probability map. This map is thresholded by a pre-determined z-score limit, and the size of the connected lesion components is computed. A lesion is detected by this algorithm with a size error

of less than 5% if the contrast ratio is at least 0.2. It may be denoted a ”true lesion” with an error probability of 5% if it is bigger than 880 voxels. Currently, we analyze temporal changes of incompletely damaged tissue in a longitudinal study.

Acknowledgements

The author wishes to thank the MPI of Human and Cognitive Brain Science, Leipzig, for providing the datasets. The help of Dr. Claire Chalopin in the development of this algorithm during her visit at MPI is greatfully acknowledged.

References

1. Abramowitz, M., Stegun, I.A. (1992) Handbook of mathematical functions with formulas, graphs, and mathematical tables. United States Department of Commerce, Washington.
2. Bello, F., Colchester, A.C.F. (1998) Measuring global and local spatial correspondence using information theory. In: Proc. MICCAI 1998, Lecture Notes in Computer Sciences **1496**, 964–973.
3. Dastidar, P., Heinonen, T., Ahonen, J., Jehkonen, M. Molnar, G. (2000) Volumetric measurements of right cerebral hemisphere infarction: use of a semiautomatic MRI segmentation technique. Comp. Biol. Med. **30**, 41–54.
4. Ho, S., Bullitt, E., Gerig, G. (2002) Level-set evolution with region competition: automatic 3D segmentation of brain tumors. In: Proc. ICPR 2002, 532–535.
5. Hojjatoleslami, S.A., Kittler, J. (1998) Region growing: A new approach. IEEE Trans. Image Proc. **7**, 1079–1083.
6. Hojjatoleslami, S.A., Kruggel, F. (2001) Segmentation of large brain lesions. IEEE Trans. Med. Imag. **20**, 666–669.
7. Kamber, M., Shinghal, R., Collins, L., Francis, G.S., Evans, A.C. (1995) Model based 3D segmentation of multiple sclerosis lesions in magnetic resonance brain images. IEEE Trans. Med. Imag. **14**, 442–453.
8. Kaus, M.R., Warfield, S.K., Nabavi, A., Black, P.M., Jolesz, F.A., Kikinis, R. (2001) Automated segmentation of MR images of brain tumors. Radiology **218**, 586–591.
9. Kruggel, F., Lohmann, G. (1996) BRIAN (brain image analysis) - a tool for the analysis of multimodal brain data sets. In: Proc. CAR 1996, 323–328.
10. Lee, J.H., Garwood, M., Menon, R., Adriany, G., Andersen, P., Truwit, C.L., Ugurbil, K. (1995) High contrast and fast three-dimensional magnetic resonance imaging at high fields. Magn. Reson. Med. **34**, 308–312.
11. Leemput, K.V., Maes, F., Bello, F., Vandermeulen, D., Colchester, A.C.F., Suetens, P. (1999) Automated segmentation of MS lesions from multi-channel MR images. In: Proc. MICCAI 1999, Lecture Notes in Computer Sciences **1679**, 11–21.
12. Loncaric, S., Dhawan, A.P., Broderick, J., Brott, T. (1995) 3D image analysis of intracerebral brain hemorrhage. Comp. Meth. & Prog. Biomed. **46**, 207–216.
13. Loncaric, S., Dhawan, A.P., Cosic, D., Kovacevic, D., Broderick, J., Brott, T. (1999) Quantitative intracerebral brain hemorrhage analysis. In: Proc. SPIE **3661**, 886–894.
14. Maksimovic, R., Stankovic, S. Milovanovic, D. (2000) Computed tomography image analysis: 3D reconstruction and segmentation applying active contour models - snakes. Int. J. Med. Info. **59**, 29–37.
15. Moon, N., Bullitt, E., van Leemput, K., Gerig, G. (2002) Model-based brain and tumor segmentation. In: Proc. ICPR 2002, 528-531.

16. Rencher, A.C. (1997) Methods of multivariate analysis. Wiley, New York.
17. Stocker, A., Sipilä, O., Visa, A., Salonen, O., Katila, T. (1996) Stability study of some neural networks applied to tissue characterization of brain magnetic resonance images. In: Proc. ICPR 1996, 472–476.
18. Tao, Y., Grosky, W.I., Zamorano, L., Jiang Z., Gong, J. (1999) Segmentation and representation of lesions in MRI brain images. In: Proc. SPIE **3661**, 930–939.
19. Velthuizen, R.P., Clarke, L.P., Phuphanich, S., Hall, L.O., Bensaid, A.M., Arrington, J.A., Greenberg, H.M., Silbiger, M.L. (1995) Unsupervised measurement of brain tumor volume on MR images. J. Magn. Reson. Imag. **5**, 594–605.
20. Willems, G., Pison, G., Rousseeuw, P.J., van Aelst, S. (2002) A robust Hotelling test. Metrika **55**, 125–138.
21. Zijdenbos, A.P., Dawant, B.M., Margolin, R.A., Palmer, A.C. (1994) Morphometric analysis of white matter lesions in MR images: method and validation. IEEE Trans. Med. Imag. **13**, 716–724.
22. Zijdenbos, A.P., Forghani, R., Evans, A.C. (1998) Automatic quantification of MS lesions in 3D MRI brain data sets: validation of insect. In: Proc. MICCAI 1998, Lecture Notes in Computer Sciences **1496**, 439–448.